Gelation in mixtures of polymers and bidisperse colloids

Rahul Pandey and Jacinta C. Conrad

Department of Chemical & Biomolecular Engineering, University of Houston, Houston, Texas 77204-4004, USA

We investigated the effects of varying the volume fraction of large particles (r) on the linear rheology and microstructure of mixtures of polymers and bidisperse colloids, in which the ratio of the small and large particle diameters was $\alpha = 0.31$ or $\alpha = 0.45$. Suspensions formulated at a total volume fraction of $\phi_T = 0.15$ and a constant concentration of polymer in the free volume $c/c^* \approx 0.7$ contained solid-like gels for small r and fluids or fluids of clusters at large r. The solid-like rheology and microstructure of these suspensions changed little with r when r was small, and fluidized only when $r > 0.8$. By contrast, dense suspensions with $\phi_T = 0.40$ and $\alpha = 0.31$ contained solid-like gels at all concentrations of large particles and exhibited only modest rheological and microstructural changes upon varying the volume fraction of large particles. These results suggest that the effect of particle-size dispersity on the properties of colloid-polymer mixtures are asymmetric in particle size and are most pronounced near a gelation boundary.

I. INTRODUCTION

Colloidal suspensions with attractive interparticle interactions are widely employed in technological processes, including inkjet printing [1,2], direct write assembly [3,4], coatings [5], catalyst synthesis [6], ceramic devices [7], drug delivery [8,9], and crude oil recovery [10–12]. The practical need to controllably tune suspension microstructural and flow properties demands a thorough understanding of the phase behavior of attractive suspensions and hence has inspired studies spanning a wide range of system parameters [13–18]. Using model systems in which the colloidal particles have a narrow size distribution, prior studies showed that the phase behavior [19–25], microstructure [15,26], and viscoelasticity [27–29] of attractive colloidal suspensions depend on the volume fraction of the colloidal particles and on the strength and range of the interparticle interactions.

By comparison, fewer fundamental studies of the phase behavior of colloidal suspensions have explored the effects of particle-size dispersity, an inherent feature of many technological suspensions. Because continuous distributions of particle size exhibiting large dispersity are difficult to realize in experiment (although accessible by theory [30,31] and/or simulation [32,33]), mixtures of particles of two different sizes are a common experimental platform in which to investigate the effects of size dispersity on phase behavior and flow properties. Important parameters controlling these properties include the volume fraction of each species and the size ratio between the particles. Most studies of phase behavior have focused on particles with hard-sphere or repulsive interactions [32,34–39]. Small particles can induce a depletion attraction [40] between large particles; the resulting interplay between the large-large and small-large interactions generates a multitude of phases, which may exhibit nonmonotonic dependence on system parameters [38,39,41]. For example, when the ratio of the radii of the small and large particles $\alpha = a_S/a_L$ is sufficiently high, suspensions can macroscopically phase separate or fractionate into regions of small and large particles [35,42]; fractionation is also theoretically predicted for continuous distributions of particle-size dispersity [43]. Similarly, decoupling of the dynamics of particles of different sizes [44] may smear out the glass transition [45] or generate distinct glassy phases [46,47].

Even fewer studies have attempted to identify effects of size dispersity on the properties of suspensions with attractive interparticle interactions. One commonly studied model for attractive suspensions consists of mixtures of nearly-hard-sphere colloidal particles and nonadsorbing polymers, in which the polymers induce an entropic depletion attraction between the particles [20]. Particle polydispersity in these mixtures shifts the equilibrium phase behavior, affecting both the number of phases and the location of boundaries between them [43,48]. Indeed, these shifts may be significant enough to reveal [49,50] or suppress [50,51] the concentrated equilibrium phases predicted for monodisperse suspensions. High particle polydispersity can also disrupt nonequilibrium phases, such as the reentrant glass transition observed at high particle concentrations [52]. At moderate total volume fraction of particles ϕ_T, however, the effects of particle polydispersity on nonequilibrium phases are not well understood. In an earlier study, we showed that changing the fraction of large particles in confined mixtures of polymers and bidisperse particles formulated at a constant total particle volume fraction $\phi_T \approx 0.15$ and at a constant ratio of the particle radii $\alpha = a_S/a_L \approx 0.49$ modified the dynamics of the large particles [53]. Broader understanding of the effects of particle-size dispersity on the bulk mechanical properties and phase behavior remains limited and is the focus of this study.

Here we show that particle size asymmetrically affects the mechanical and microstructural properties of mixtures of polymers and slightly bidisperse colloids. For suspensions with moderate total volume fraction ($\phi_T = 0.15$), fixed particle-size ratio ($\alpha = 0.31$), and a fixed and large concentration of depletant polymer in the free volume accessible to the polymer centroid ($c/c^* \approx 0.7$), we observed a transition from solid-like to fluid-like behavior as the volume fraction of the large particles ($r = \phi_L/\phi_T$) was increased from 0 to 1. Adding a minor amount of large particles to a suspension of small particles (near $r = 0$) negligibly affected the linear rheology and microstructure, whereas adding a minor amount of small particles to a suspension of large particles (near $r = 1$) generated more significant changes in these properties. When the size ratio was increased ($\alpha = 0.45$) while ϕ_T was held

constant, similar evolution of the rheology and microstructure was seen upon increasing volume fraction of large particles. By contrast, increasing the total volume fraction of particles to $\phi_T = 0.40$ largely mitigated the dispersity-induced changes in rheology and microstructure. The gel networks present for $r = 0$ weakened slightly upon increasing volume fraction of large particles but did not become fluid. We speculate that these changes arise from the decrease in the effective range of the interparticle attraction as the volume fraction of large particles is increased. The location of the gelation boundary depends on the range of the attraction [22,24,25] as well as the particle and polymer concentrations. At moderate $\phi_T = 0.15$, a small decrease in the attraction range shifts the gelation boundary to greater polymer concentration; as a result, the suspension becomes more fluid as the small particles are replaced by large particles. Conversely, at $\phi_T = 0.40$ the suspension is deeply quenched, far from the gelation boundaries of both small and large particles; hence, changes in their volume ratio only minimally affect the rheology and microstructure. These findings suggest that the effects of particle-size dispersity on the rheology and microstructure of attractive suspensions are more pronounced near a fluid-solid phase boundary.

II. MATERIALS AND METHODS

A. Sample preparation

Poly(methyl methacrylate) (PMMA) particles were synthesized and sterically stabilized with poly(12-hydroxystearic acid) [54]. The diameter and polydispersity of each particle batch were characterized using dynamic light scattering (BI-APD). Next, particles were suspended in a solvent mixture of cyclohexylbromide (CXB, Sigma-Aldrich) and decahydronaphthalene (DHN, Sigma-Aldrich) at a weight ratio of 3:1, which approximately matched both the density ($\rho \approx 1.21$ g/ml) and index of refraction ($n \approx 1.49$) of the particles. A monovalent salt, tetrabutylammonium chloride (TBAC, Sigma-Aldrich, purum), was added to all mixtures at an oversaturated concentration of 1.5 mM to partially screen the electrostatic charge on the particles and hence reduce long-range repulsions. To induce interparticle attractions, non-adsorbing linear polystyrene ($M_w = 299{,}800$ Da, $M_w/M_n = 1.05$, Agilent Technologies) was added to all samples at a fixed concentration of polymer in the free volume $c_p = 25$ mg/ml. The radius of gyration of polystyrene was $R_g = 15$ nm and the overlap concentration was $c_p^* = 3M_w/4\rho R_g^3 N_A \approx 35$ mg/ml. The range of the depletion attraction between particles is controlled by the ratio of the radius of gyration of the polystyrene polymer to the particle radius $\xi = R_g/a$. For all particles used in this study the range of the interparticle attraction was $\xi < 0.06$, corresponding to a short-ranged attraction. (Estimates of the interparticle interactions are presented in the Appendix.) To minimize sedimentation due to gravity, we confirmed that particles remained suspended after centrifugation at 800 g and $25°$C for 75 min; as needed, drops of CXB or DHN were added to improve the buoyancy matching. Samples were allowed to equilibrate for 24 h before rheological measurements or before loading into sample chambers for imaging experiments.

TABLE I. Particle sizes, size ratio α, total volume fraction ϕ_T, and effective ranges of attraction for the three model suspensions used in this study.

	Series 1	Series 2	Series 3
$2a_S$ [μm] (PDI [%])	0.54 (6.7)	0.71 (5.1)	0.54 (6.7)
$2a_L$ [μm] (PDI [%])	1.76 (5.6)	1.57 (3.5)	1.76 (5.6)
$\alpha = a_S/a_L$	0.31	0.45	0.31
Total volume fraction ϕ_T	0.15	0.15	0.40
$\xi_S = R_g/a_S$	0.055	0.042	0.055
$\xi_L = R_g/a_L$	0.017	0.019	0.017

We investigated three different combinations of the ratio of the radii of the small and large particles, $\alpha = a_S/a_L$, and the total volume fraction $\phi_T = \phi_L + \phi_S$, where ϕ_L and ϕ_S were the volume fractions of large and small particles, respectively (Table I). Large particles (of diameter $2a_L = 1.76$ μm or $2a_L = 1.57$ μm) were labeled with the fluorescent dye Rhodamine B (Sigma-Aldrich) and small particles (of diameter $2a_S = 0.54$ μm or $2a_S = 0.71$ μm) were fluorescently labeled with Fluorescein 5(6)-isothiocyanate (FITC, Sigma-Aldrich). For each combination of α and ϕ_T, we varied the volume fraction of large particles $r = \phi_L/\phi_T$ from 0 to 1 and investigated a series of samples with $r = 0.0$, 0.50, 0.75, 0.87, 0.93, 0.96, and 1.0; for large-particle dynamic experiments we also investigated a sample with $r = 0.1$.

B. Rheological measurements

Dynamic rheology measurements were performed using a TA hybrid rheometer (TA Discovery HR2) equipped with a Couette cell geometry. The gap size was 1.19 mm and the bob length was 41.89 mm. All measurements were performed at a constant temperature of $25°$C that was maintained by a circulating coolant jacket. As shear history is known to affect the microstructural and rheological properties of samples [55], prior to each rheological measurement samples were presheared at 100 s^{-1} for 1 min and then allowed to equilibrate for 1200 s, beyond which the elastic modulus did not significantly increase. We first determined the linear viscoelastic regime for each sample by measuring the elastic (G') and viscous (G'') moduli as a function of the stress amplitude σ at a fixed frequency of $\omega = 10^{-2}$ Hz, 10^{-1} Hz, and 10^0 Hz. We subsequently measured G' and G'' as a function of frequency over the range 10^{-3} Hz $< \omega < 10^1$ Hz at a fixed stress amplitude of 2×10^{-4} Pa for suspensions with $\phi_T = 0.15$ or 1×10^{-3} Pa for suspensions with $\phi_T = 0.40$; these choices ensured that the sample remained in the linear viscoelastic regime across the range of frequencies probed for each sample.

C. Confocal microscopy

Samples were imaged using a confocal point-scanner (VT-Eye, VisiTech International) that was attached to an inverted microscope (Leica DMI3000B). The confocal microscope was equipped with two laser sources with wavelengths $\lambda = 491$ nm and $\lambda = 561$ nm. The $\lambda = 491$-nm wavelength excited both fluorescent dyes; a 500-nm long-pass barrier filter was used to simultaneously image both small and

large particles, and a 525- to 550-nm barrier bandpass filter was used to preferentially (but not exclusively) image the FITC-labeled small particles. The $\lambda = 561$-nm line excited only the rhodamine dye and was used to selectively image the large particles. Samples loaded into rectangular chambers of thickness 1 mm that were fabricated from coverslips (Gold Seal) were allowed to rest undisturbed for 30 min before imaging experiments. To investigate the dynamics of the particles, we sequentially acquired multiple two-dimensional (2D) movies (x-y) at a constant height of 60 μm above the bottom surface of the chamber. Each 2D movie consisted of 500 8-bit images acquired at a rate of 1 frame/s. To characterize the microstructure of the suspensions, we acquired three-dimensional (3D) image stacks of total thickness 50 μm, acquired in a region of the sample that was between 10 and 60 μm above the bottom of the chamber. Individual 2D images in 3D stacks were spaced by a distance of $\Delta z = 0.1$ μm and were acquired at an acquisition rate of 31.7 frames/s to capture the microstructure at a given time. We used standard particle-tracking algorithms to locate the positions of large particles in 3D and track the positions of large particles in 2D (x-y) over time [56]. We were unable to locate the centroids of the small particles, because the $\lambda = 491$-nm line also excited the dye used to label the large particles. The resolution of our particle tracking algorithm was $\sim$40 nm, as measured by the y intercept of the mean-square displacement as a function of time in dilute suspensions.

III. RESULTS AND DISCUSSION

A. Series 1 ($\phi_T \approx 0.15$ and $\alpha \approx 0.31$)

We first characterized the properties of a series of suspensions with $\phi_T \approx 0.15$ and $\alpha \approx 0.31$ as the volume fraction r of large particles was increased. To quantify the change in linear viscoelasticity of the suspensions with increasing large particle fraction, we measured the elastic [$G'(\omega)$] and viscous [$G''(\omega)$] moduli as a function of frequency ω. The elastic modulus of a suspension containing only small particles ($r = 0$) was nearly independent of frequency [Fig. 1(a)], as expected for a weak elastic solid. As r was increased, the elastic modulus became increasingly dependent on frequency and the magnitude of G' decreased; both changes are consistent with weakening of the solid. A suspension containing only large particles [$r = 1.0$, Fig. 1(f)] behaved as a viscoelastic fluid, with $G' \leqslant G''$ across the range of frequencies measured. The evolution from weak solid to viscoelastic fluid occurred nonuniformly with r, as shown by examining the value of G' at a fixed frequency $\omega = 10^{-2}$ Hz. As r was increased from 0 to 0.75, the elastic modulus decreased by approximately one order of magnitude; upon further increasing r from 0.75 to 1, however, the elastic modulus decreased by two orders of magnitude. This result indicated that the evolution of the linear rheology occurred asymmetrically in particle size.

To connect the bulk rheology to local properties, we characterized the suspension dynamics and microstructure as a function of r using confocal microscopy. We first quantified the dynamics of the large particles in the suspensions via the 1D mean-square displacement (MSD), $\langle \Delta x^2(\tau) \rangle$, to confirm the increasingly fluid-like behavior of the suspensions observed in
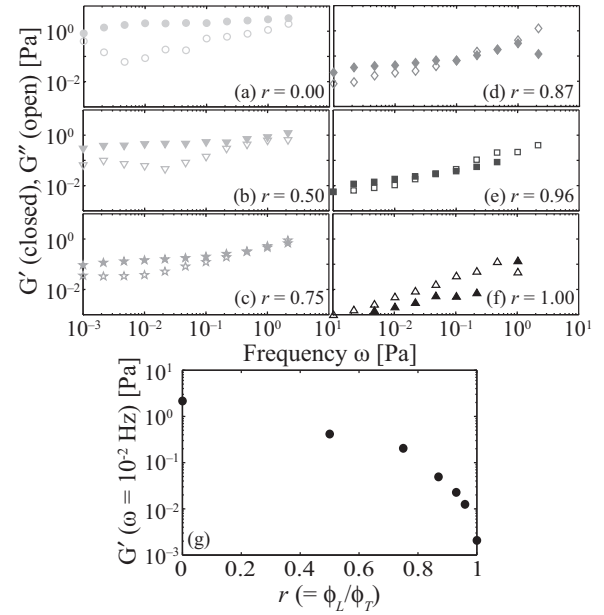

FIG. 1. (a)–(f) Storage (G', closed symbols) and loss (G'', open symbols) moduli as a function of frequency (stress amplitude $= 2 \times 10^{-4}$ Pa) for suspensions with total volume fraction $\phi_T \approx 0.15$, polymer concentration $c_p = 25$ mg/ml, and particle size ratio $\alpha \approx 0.31$. Volume fraction of large particles r: (a) 0.00, (b) 0.50, (c) 0.75, (d) 0.87, (e) 0.96, (f) 1.00. (g) Elastic modulus at a frequency of 10^{-2} Hz, $G'(\omega = 10^{-2}$ Hz), as a function of r.

the rheological experiments. A suspension containing mostly small particles ($r = 0.10$) exhibited strongly subdiffusive dynamics, as shown in Fig. 2. As r was increased, both the magnitude and slope of the MSD increased, consistent with increasingly diffusive and fluid-like dynamics. Even at $r = 1.0$, however, the slope of the MSD was less than 1, consistent with the dynamics expected for a dense fluid. The evolution of large-particle dynamics from arrested at $r = 0.1$ to nearly diffusive at $r = 1.0$ was consistent both with the solid-to-fluid transition and with the asymmetry in r observed
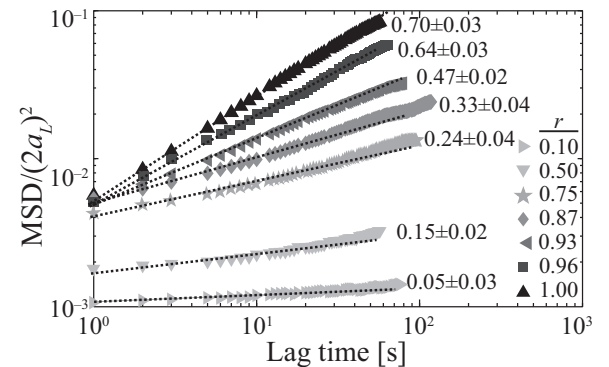

FIG. 2. Normalized mean-squared displacement MSD/$(2a_L)^2$ as a function of lag time τ for large particles in suspensions with total colloid volume fraction $\phi_T \approx 0.15$, polymer concentration $c_p = 25$ mg/ml, and particle size ratio $\alpha \approx 0.31$ but varying volume fraction of large particles r. The dashed lines indicate power-law fits (MSD $\sim \tau^\beta$), with the exponents β reported next to each fit.
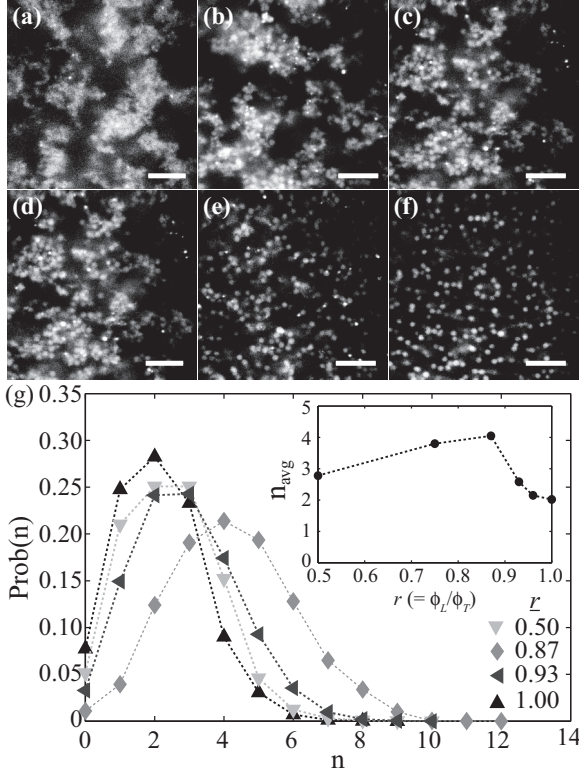
FIG. 3. (a)–(f) Confocal micrographs of small and large particle populations for suspensions with total volume fraction $\phi_T \approx 0.15$, polymer concentration $c_p = 25$ mg/ml, particle size ratio $\alpha \approx 0.31$, and volume fraction of large particles r of (a) 0.00, (b) 0.50, (c) 0.75, (d) 0.87, (e) 0.93, and (f) 1.00. The scale bar is 10 μm. (g) Probability distribution of the number of large-large particle bonds. Inset: Average bond number n_{avg} as a function of r.

in the bulk rheology; the slope of the MSD increased only modestly from $r = 0.1$ to $r = 0.5$ but increased markedly above $r > 0.75$.

The microstructure of the suspension evolved from a connected network to a disconnected fluid as r was increased, as shown in Fig. 3. A suspension of small particles ($r = 0$) contained an interconnected and heterogeneous network consisting of clusters of particles, consistent with a solid-like colloidal gel [57]. At intermediate r [e.g., $r = 0.50$, Fig. 2(b), or $r = 0.75$, Fig. 2(c)] the small and large particles together formed a percolating network. At $r = 0.87$ the percolating network was lost, and the suspension instead contained a homogeneous mixture of mobile clusters of particles and free particles. At $r = 1.0$ the large particles were dispersed and formed a dense fluid.

As one measure of the local microstructure, we characterized the probability distribution of the number of large-large particle bonds. We defined the first minimum in the pair distribution function $g(r)$ as the maximum cutoff distance for a particle-particle bond and hence calculated the number of large-particle bonds for each large particle. The resulting probability distribution of bond number (n) was approximately described by a Gaussian function and exhibited a local maximum for all concentrations, as shown in Fig. 3(g). The average number of large-large bonds n_{avg}, which approximately

corresponded to the position of the maximum, first shifted to higher n as r was increased to $r = 0.87$, consistent with the increasing number of large particles, and then decreased as r was further increased to $r = 1.0$. For $r > 0.87$ the suspension exhibited fluid-like rheology [i.e., $G'' \geqslant G'$, as shown in Figs. 1(e) and 1(f)], suggesting that the loss of large-large particle bonds occurs concomitant with increased fluidity.

In summary, the weak solid gel present at $r = 0$ gradually fluidized as the volume fraction of large particles r was increased, as indicated by the decrease in magnitude of G' at a fixed frequency and the increase in the magnitude and slope of the MSD. Changes in properties did not occur uniformly with increasing r; instead, the suspensions first gradually became less solid-like over a broad range of r ($0 \leqslant r \leqslant 0.87$) but then more rapidly became fluid-like over the remaining narrow range of r ($0.87 \leqslant r \leqslant 1$). The number of large-large particle bonds exhibited a local maximum at an intermediate value of $r = 0.87$, above which the suspension rheology was fluid-like.

B. Series 2 ($\phi_T \approx 0.15$ and $\alpha \approx 0.45$)

We next formulated a series of suspensions at the same total volume fraction ($\phi_T \approx 0.15$) but a greater particle size ratio $\alpha \approx 0.45$. The changes in the elastic and viscous moduli with r in this series were qualitatively similar to those observed in the suspensions with $\alpha \approx 0.31$. The value of the elastic modulus G', measured at a frequency $\omega = 10^{-2}$ Hz and a stress amplitude $\sigma = 2 \times 10^{-4}$ Pa, again gradually decreased with increasing large particle volume fraction until $r = 0.87$ and then decreased sharply with further increases in r [Fig. 4(a)]. These findings indicated that a small change in the particle-size ratio did not qualitatively alter the evolution of the mechanical properties.

Likewise, the trends in microscale dynamics and structure were qualitatively similar to those observed for $\alpha \approx 0.31$. All suspensions exhibited subdiffusive dynamics, and both the magnitude and slope of the MSD of large particles increased as r was increased [Fig. 4(b)]. The average number of large particle-large particle bonds again depended nonmonotonically on r, with the maximum number of bonds n_{ave} observed at $r = 0.87$ [Fig. 4(c)]. Notably, although the volume fraction of large particles at the maximum of n_{ave} ($r = 0.87$) was constant for Series 1 and Series 2 suspensions, the number ratio of large and small particles was not: for $\alpha = 0.31$ the ratio of the number of large to small particles was $N_L/N_S \approx 0.20$ (i.e., approximately five small particles for every one large), whereas for $\alpha = 0.45$ $N_L/N_S \approx 0.62$ (i.e., approximately five small particles for every three large).

The evolution of mechanical and microstructural properties with r for Series 2 ($\alpha = 0.45$) exhibited some quantitative differences from that observed for Series 1 ($\alpha = 0.31$). Compared to $\alpha = 0.31$, the order of magnitude of the change in the elastic modulus at $\alpha = 0.45$ was smaller and suspensions remained weakly gelled even at $r = 1.0$; these changes are likely due to the smaller radius of the large particles used in the $\alpha = 0.45$ series of experiments. Similarly, at a given r the number of large-large particle bonds was slightly larger for the $\alpha = 0.45$ series of samples. Variability in the surface charge on fluorescently dyed PMMA particles [58] can modify the effective interparticle potential [59], making quantitative
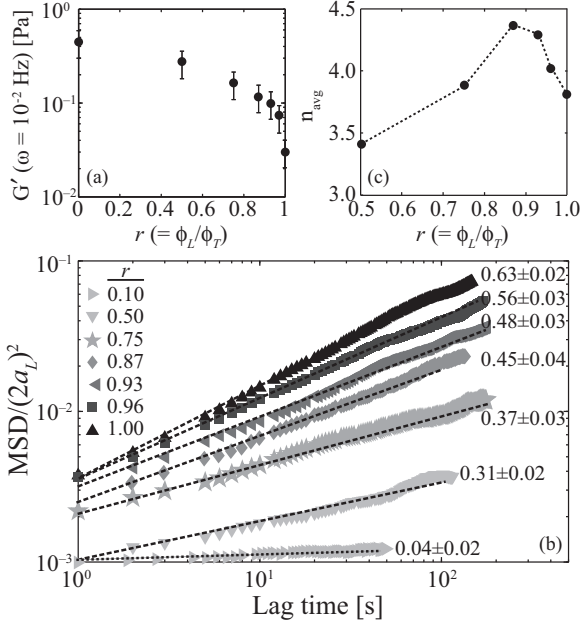
FIG. 4. Summary of mechanical, dynamic, and microstructural characterizations for suspensions with $\phi_T \approx 0.15$, polymer concentration $c_p = 25$ mg/ml, and particle size ratio $\alpha \approx 0.45$. (a) Elastic modulus at a fixed frequency $\omega = 10^{-2}$ Hz as a function of volume fraction of large particles r. (b) Normalized mean-squared displacement MSD/$(2a_L)^2$ as a function of lag time τ for large particles. The dashed lines indicate power-law fits (MSD $\sim \tau^\beta$), with the exponents β reported next to each fit. (c) Average bond number n_{avg} as a function of r.

comparisons between series of experiments using different batches of particles difficult. Nonetheless, the measurements reported in Fig. 4 suggested that the qualitative features of the gradual fluidization were not sensitive to small changes in the size ratio α.

C. Series 3 ($\phi_T \approx 0.40$ and $\alpha \approx 0.31$)

Finally, we formulated a series of suspensions with particle size ratio of $\alpha \approx 0.31$, as in the first series of samples (Sec. III A), and greater total volume fraction $\phi_T \approx 0.40$. For all values of r these suspensions behaved like elastic gels, with $G'(\omega) > G''(\omega)$ at low frequencies as shown in Fig. 5. The elasticity did not significantly decrease with r, in contrast to the striking fluidization observed for samples formulated at lower ϕ_T (Secs. III A and III B). Here, the low-frequency elastic modulus $G'(\omega = 10^{-2}$ Hz) decreased by about one order of magnitude as r was increased from 0 to 1, significantly less than the three-order-of-magnitude decrease observed in Series 1 ($\phi_T \approx 0.15$).

All samples formulated with $\phi_T \approx 0.40$ exhibited arrested microscopic dynamics, consistent with their macroscopic elasticity. The slope of the MSD was close to zero for all values of r studied, as shown in Fig. 6, and within the resolution of our measurements did not change with r. The magnitude of the MSD increased very slightly with increasing r, consistent with the slight weakening of the network also observed in the bulk rheological measurements in Fig. 6.
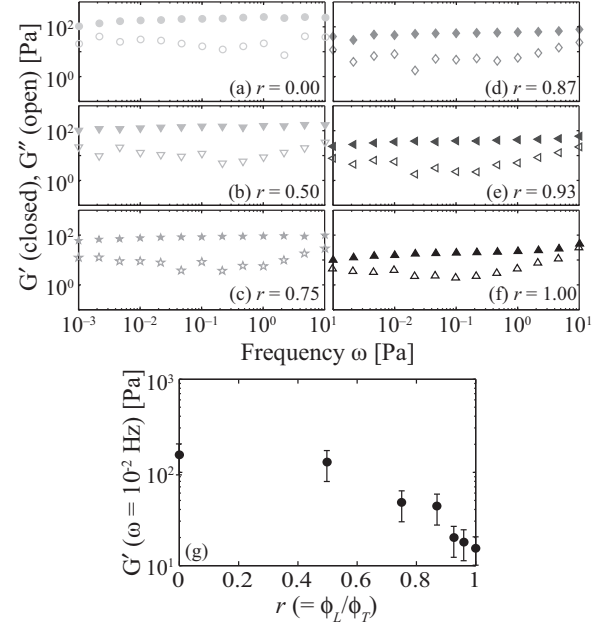

FIG. 5. (a)–(f) Storage (G', closed symbols) and loss (G'', open symbols) moduli as a function of frequency (stress frequency = 1×10^{-3} Pa) for suspensions with total volume fraction $\phi_T \approx 0.40$, polymer concentration $c_p = 25$ mg/ml, and particle size ratio $\alpha \approx 0.31$. Volume fraction of large particles r: (a) 0.00, (b) 0.50, (c) 0.75, (d) 0.87, (e) 0.93, (f) 1.00. (g) Elastic modulus at a frequency of 10^{-2} Hz, $G'(\omega = 10^{-2}$ Hz), as a function of r.

The network structure did not significantly change as r was increased: confocal micrographs revealed that all suspensions contained a dense and connected network of particles, as shown in Fig. 7. The average number of large-large bonds, however, increased uniformly with r [Fig. 7(g)], in contrast to the nonmonotonic behavior of n_{avg} reported for suspensions with $\phi_T \approx 0.15$. This result is consistent with the gradual replacement of small particles by large particles without a change in the phase behavior of the suspension.
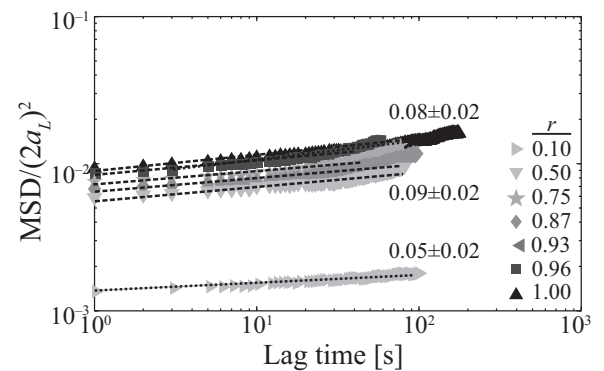

FIG. 6. Normalized mean-squared displacement MSD/$(2a_L)^2$ as a function of lag time τ for large particles in suspensions with total colloid volume fraction $\phi_T \approx 0.40$, concentration of polymer $c_p = 25$ mg/ml, and particle-size ratio $\alpha \approx 0.31$ but varying volume fraction of large particles r. The dashed lines indicate power-law fits (MSD $\sim \tau^\beta$). Typical exponents β are reported near representative fit lines.
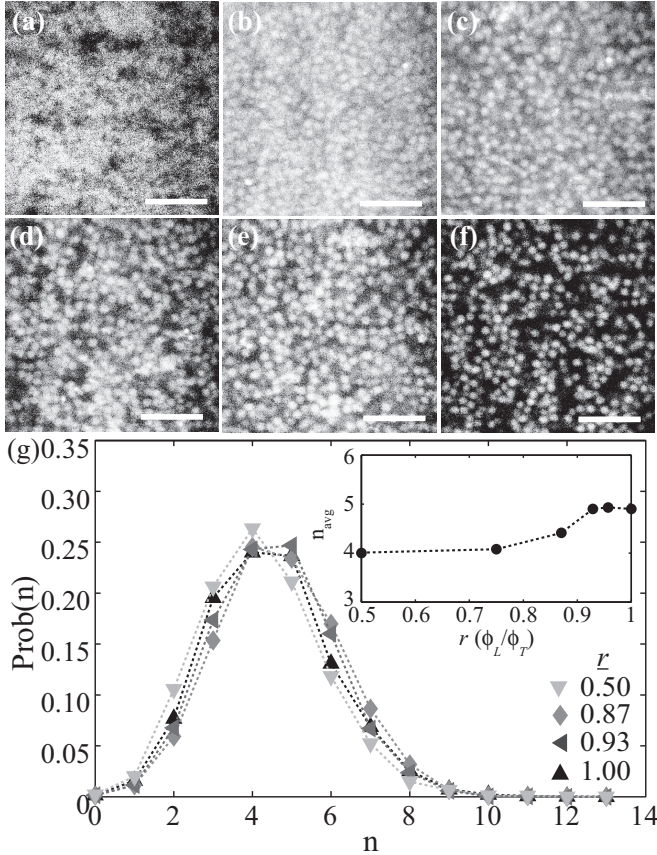
FIG. 7. (a)–(f) Confocal micrographs of small- and large-particle populations for suspensions with total volume fraction $\phi_T \approx 0.40$, polymer concentration $c_p = 25$ mg/ml, particle-size ratio $\alpha = a_S/a_L = 0.31$, and varying volume fraction of large particles r of (a) 0.00, (b) 0.50, (c) 0.75, (d) 0.87, (e) 0.93, and (f) 1.00. The scale bar is 10 μm. (g) Probability distribution of the number of large-large particle bonds. Inset: Average bond number $n_{\rm avg}$ as a function of r.

D. Discussion

We investigated the effect of varying the volume fraction of large particles r on the rheology and microstructure of mixtures of polymers and bidisperse colloids. In suspensions formulated at an intermediate total volume fraction ($\phi_T = 0.15$), the rheological, dynamic, and microstructural properties of the suspensions became less solid-like and more fluid-like as r was increased, with changes in these properties occurring gradually at small r and more rapidly only at large r. By contrast, dense suspensions with $\phi_T = 0.40$ were solid-like gels at all r and exhibited only modest rheological and microstructural changes as r was varied, as summarized in Fig. 8.

The asymmetric and nonuniform variations with r of the rheological and microstructural properties are qualitatively similar to those noted in earlier studies of the rheology [34,38] and phase behavior [39] of binary hard sphere PMMA suspensions. At a constant total volume fraction $\phi_T \approx 0.65$ and a particle size ratio $\alpha \approx 0.15$, replacing a minor fraction of large particles with small particles (r near 1) significantly altered the low-shear storage modulus; by contrast, replacing a minor fraction of small particles with large particles
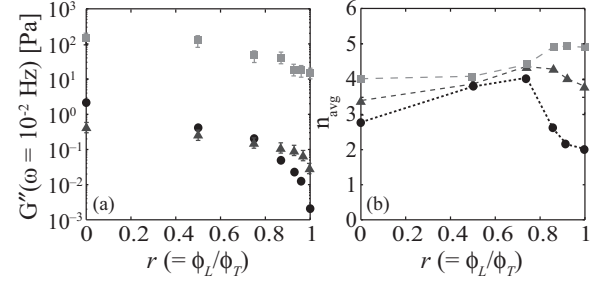

FIG. 8. Summary of metrics for mechanical and structural changes with dispersity ratio. (a) Elastic modulus at a frequency of 10^{-2} Hz, $G'(\omega = 10^{-2}$ Hz) and (b) average bond number $n_{\rm avg}$ as a function of volume fraction of large particles r for all three series of experiments: Series 1 ($\phi = 0.15$ and $\alpha = 0.31$, circles), Series 2 ($\phi = 0.15$ and $\alpha = 0.45$, triangles), and Series 3 ($\phi = 0.40$ and $\alpha = 0.31$, squares).

(r near 0) produced little change in these metrics [34]. This asymmetry in rheology was attributed to the deformation of the steric stabilizing layer on the surface of the particles [34]. In highly size-asymmetric mixtures of large and small particles ($\alpha = 0.1$–0.2) formulated at a constant total volume fraction $\phi \approx 0.6$, distinct repulsive glass and asymmetric glass states were observed at the extreme compositional ratios [38,39]. Changes in dynamics, localization length, and cluster sizes were attributed to depletion interactions induced by the small particles [39]; these microstructural changes were in turn reflected in the ratio of the elastic and viscous moduli in the linear viscoelastic regime [38]. Although asymmetric and nonuniform changes in properties that depend on particle size also appear in our system, the underlying mechanism in our system must be different, as the PS polymer induces an entropic depletion attraction between particles and leads to the formation of interparticle bonds.

To understand the origin of the changes in rheology and microstructure with r in our depletion mixtures, we considered the number and strength of the bonds between particles. First, we calculated the ratio of the numbers of large and small particles, N_L/N_S, reported in Table II. We note that the number ratio is identical for Series 1 ($\phi = 0.15$) and 3 ($\phi = 0.40$) experiments, but the trends in fluidization in these experiments do not coincide—in Series 1, the samples fluidized as r was increased but remained solids for all r in Series 3. A simple scaling argument suggests that the elastic modulus of monodisperse colloidal gels scales as the interaction

TABLE II. Number ratio of large to small particles N_L/N_S as a function of volume fraction of large particles r for Series 1, 2, and 3 experiments.

r	Series 1	Series 2	Series 3
0.10	3.2×10^{-3}	1.0×10^{-3}	3.2×10^{-3}
0.50	2.9×10^{-2}	9.2×10^{-2}	2.9×10^{-2}
0.75	8.7×10^{-2}	2.8×10^{-1}	8.7×10^{-2}
0.87	1.9×10^{-1}	6.2×10^{-1}	1.9×10^{-1}
0.93	3.8×10^{-1}	1.2×10^{0}	3.8×10^{-1}
0.96	6.9×10^{-1}	2.2×10^{0}	6.9×10^{-1}

potential U between the particles normalized by the particle radius a, i.e., as U/a^3. Hence, we estimated the effective interparticle potential between two large particles and two small particles as the sum of a screened Coulomb repulsion [60] due to the slight electrostatic charge on the particles [58] and a depletion attraction [19] induced by the polymers. (Details are given in our earlier publication [53] and in the Appendix; here we include a volume fraction correction to account for the concentration of particles in each suspension.) The interaction potentials between two large or two small particles exhibited strong attractive minima at contact, with a depth of $-60\ k_{BT}$ (large-large) or $-10\ k_{BT}$ (small-small) for suspensions with total volume fraction $\phi_T \approx 0.15$ and particle-size ratio $\alpha \approx 0.31$. The bonds between small particles are weaker than those between large particles, but not strongly so; hence the dominant effect on the gel elasticity is the change in particle size. The decrease in the elasticity of the gel networks is approximately consistent with that expected from the change in the particle size (i.e., in Series 3 G_S' is larger by about a factor of ten than G_L', and $(a_L/a_S)^3 \approx 34$) but again the fluidization cannot be explained by a gel scaling argument. Finally, small particles themselves are expected to enhance the depletion attraction between the large particles [39,61]. It is therefore unlikely that the fluidization with increasing fraction of large particles originates from a change in the number or strength of the bonds between the particles.

Instead, we considered the effect of changing the range of the interparticle attraction on the nonequilibrium phase diagram. Increasing the size of the particles while holding the size of the polymer fixed decreases the range of the interparticle attraction, parameterized by $\xi = R_g/a$. In our experiments ξ decreases as small particles are replaced by large particles and r is increased; values of the effective range of attraction for small (ξ_S) and large (ξ_L) are given in Table I. Earlier studies [22,24,25] showed that the fluid-to-solid gelation boundary for samples formulated at intermediate volume fractions shifts upward to higher polymer concentrations as ξ decreases [62]. Hence, we suggest that changes in suspension rheology and structure in our bidisperse mixtures arise from changes in the range of the effective interparticle attraction. At moderate volume fraction ($\phi_T \approx 0.15$), the nonequilibrium phase behavior of gelation is a strong function of the range of the interparticle attraction $\xi = R_g/a$ [22,25,63]. As small

particles are replaced by large particles, the fluid-to-solid gelation line moves to a higher concentration of polymer and hence a suspension that is located sufficiently close to the gelation boundary can fluidize upon decreasing the range of attraction. In an earlier study, we found that the gelation boundary for a suspension of particles of diameter 0.865 μm at a volume fraction $\phi = 0.15$ was located at approximately 20 mg/ml [64]; given that the large particles in the current experiments have diameters of 1.57 or 1.76 μm, we expect the gelation boundary to be shifted to slightly higher concentrations of polymer. In further support of the idea that the suspension formulated at $\phi_T \approx 0.15$ is initially close to a gelation boundary, we note that the linear rheology measurements for $r = 0$ [Fig. 1(a)] show that G'' depends on frequency at the lowest measurable frequencies. This frequency dependence signals an incipient crossover (i.e., $G' \approx G''$) at low frequency, consistent with relaxation on somewhat longer time scales. The rheological behavior is thus consistent with the idea that this sample is not deeply quenched into the gel.

To quantify the change in the effective range of attraction, we examined the localization length x_{loc} of the large particles. As we never observed a time-independent plateau in most of the dynamic MSD measurements, we instead estimated the localization length of the arrested particles following the protocol of Ref. [65]; in earlier experiments on PMMA particles, the localization lengths estimated from the MSD and from the protocol of Ref. [65] were very similar for fully arrested particles [15]. Briefly, we first calculated the van Hove distributions $G_S(\Delta x, \tau)$ at a fixed lag time of $\tau = 50$ s. We then calculated the normalized deviation of the van Hove distributions from the expected Gaussian value for a freely-diffusing particle [15], $(G_S(\Delta x, \tau) - G_{S,G}(\Delta x, \tau))/G_{S,G}(\Delta x, \tau)$, as shown in Fig. 9. The smallest Δx for which the deviation function equalled zero provided an estimate of the localization length x_{loc}, shown in the inset in each panel in Fig. 9. For all samples the particles became slightly less localized as r was increased, consistent with an increasing effective ξ. Mode-coupling theory predicts that $G' \propto x_{\text{loc}}^{-2}$ (Ref. [66]), and hence this increase of the localization length with increasing r is consistent with the decrease in elasticity in each sample, as observed earlier for monodisperse colloidal gels [67].

Following our argument, the lack of evolution of the mechanical and dynamic properties of suspensions formulated
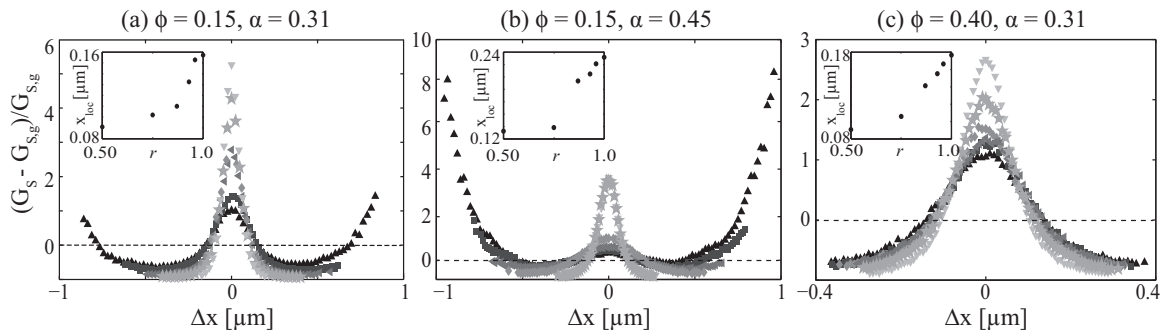

FIG. 9. Normalized deviation of the van Hove correlation function from the Gaussian function for single-particle displacements, $(G_S(\Delta x, \tau) - G_{S,G}(\Delta x, \tau))/G_{S,G}(\Delta x, \tau)$ at a lag time $\tau = 50$ sec for (a) $\phi_T \approx 0.15, \alpha \approx 0.31$; (b) $\phi_T \approx 0.15, \alpha \approx 0.45$; (c) $\phi_T \approx 0.40$, $\alpha \approx 0.31$. Inset: localization length x_{loc} extracted from the first zero of $(G_S(\Delta x, \tau) - G_{S,G}(\Delta x, \tau))/G_{S,G}(\Delta x, \tau)$ as a function of the volume fraction of large particles r.

at $\phi_T \approx 0.40$ suggests that these suspensions are located far from any fluid-to-solid gelation boundary. Here we suggest that these suspensions are deeply quenched into the gel phase, based on the nearly frequency-independent elastic modulus (Fig. 5) and the nearly time-independent MSD (Fig. 6). Although changing the range of attraction via r may shift the effective location of a sample in phase space [as indicated by the weakening of the elastic network and the increase in the localization length in Fig. 9(c)], this change is not sufficient to fluidize the gel network.

IV. CONCLUSION

We investigated changes in rheology and microstructure in mixtures of polymers and bidisperse colloids as the volume fraction of large particles was increased. The extent of changes in these properties depended on the total volume fraction ϕ_T but not on the size ratio between large and small particles α (across the narrow range accessed here). Suspensions formulated at intermediate $\phi_T \approx 0.15$ that were solid-like at $r = 0$ became more fluid-like as r was increased. The fluidization was asymmetric in r; dramatic changes in mechanics or structure occurred only when the large particles constituted a significant fraction of the volume of total particles (i.e., at large values of r). By contrast, suspensions formulated at a higher total volume fraction of $\phi_T \approx 0.40$ were elastic gels at all r and exhibited only modest rheological and microstructural changes as r was increased. To explain these changes, we posit that changes arise from a decrease in the effective range of attraction ξ with increasing r combined with proximity to a gelation boundary. Near the gelation boundary a slight change in ξ may be sufficient to change the overall phase behavior; far from the boundary (i.e., for a deeply quenched sample) a slight change in ξ is insufficient to alter the nonequilibrium phase behavior. This study hence suggests that the effects of size dispersity on the properties of colloid-polymer mixtures are most pronounced near the boundary of a fluid-solid gelation transition.

Colloidal suspensions used in technological applications often contain particles of a broad range of sizes. As a result, fundamental understanding of the effects of particle-size dispersity is required to formulate technological suspensions with controlled properties for use in applied settings. Here, we report that changes of the properties of attractive suspensions with particle dispersity are asymmetric in the particle size, consistent with earlier studies of colloidal particles with repulsive interparticle interactions [34]. In our system adding a small fraction of large particles to a suspension of attractive small particles does not significantly alter suspension properties or phase behavior, whereas adding a small fraction of small particles may be sufficient to generate a colloidal solid in the vicinity of a nonequilibrium solidification boundary. Translating these mechanistic insights into predictive models requires detailed studies of the microstructure and mechanics as a function of the distance from phase boundaries; model systems [68] and measurement techniques [69] that enable simultaneous characterization of rheology and microstructure are expected to provide further insight into the role of particle polydispersity on suspension properties. Finally, our study focused on the quiescent phase behavior and linear flow

properties, whereas applications frequently involve nonlinear deformations. Particle-size dispersity is known to alter the viscosity and yielding of hard-sphere suspensions [34,70] and we expect that it will also significantly modify the viscosity of attractive suspensions.

APPENDIX: CALCULATION OF INTERACTION POTENTIALS

We estimated the interaction potential between two similarly sized PMMA particles (either large-large or small-small) as the sum of electrostatic and depletion contributions,

$$\frac{U}{k_B T} = \frac{U_{ES}}{k_B T} + \frac{U_{dep}}{k_B T}, \qquad (A1)$$

where k_B is Boltzmann's constant and T is the temperature. The results of the calculations are presented in Fig. 10 and a detailed discussion of the parameters and assumptions used in
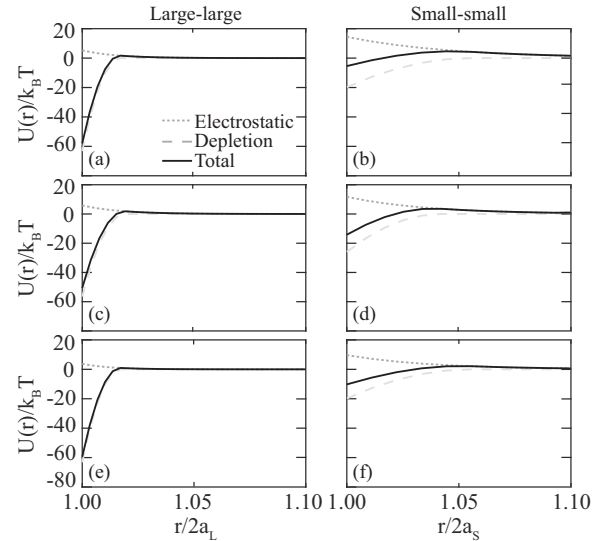

FIG. 10. Dimensionless electrostatic (dotted lines), depletion (dashed lines), and overall (solid lines) between spherical particles as a function of the normalized interparticle distance $r/2a_L$ (for large particles, (a), (c), (e)) or $r/2a_S$ (for small particles, (b), (d), (f)) for polymer concentration $c_p = 25$ mg/ml. (a), (b): Series 1 experiments: $\phi = 0.15$ and $\alpha = a_S/a_L = 0.31$ ($2a_L = 1.76$ μm or $2a_S = 0.54$ μm); (c), (d): Series 2 experiments: $\phi = 0.15$ and $\alpha = a_S/a_L = 0.45$ ($2a_L = 1.57$ μm or $2a_S = 0.71$ μm); (e), (f): Series 3 experiments: $\phi = 0.40$ and $\alpha = a_S/a_L = 0.31$ ($2a_L = 1.76$ μm or $2a_S = 0.54$ μm).

these calculations follows. First, to estimate the electrostatic interactions, we used a screened Coulomb potential to describe the electrostatic interaction [$U_{ES}(r)$] as a function of the center-to-center separation r in the presence of the quaternary ammonium salt TBAC. The screened Coulomb potential can be written as [71]

$$\frac{U_{\mathrm{ES}}(r)}{k_B T} = \left(\frac{e\zeta}{k_B T}\right)^2 \frac{a^2}{\lambda_B} \frac{e^{-\kappa(r-2a)}}{r}, \qquad \text{(A2)}$$

where e is the electron charge, ζ is the zeta potential of the particles in the CHB:DXN solvent mixture, a is the particle radius, λ_B is the Bjerrum length, and κ^{-1} is the Debye screening length. The Debye screening length was estimated as [72]

$$\kappa^2 = \frac{e^2 z^2}{\epsilon k_B T} \frac{2\rho + \frac{3\sigma\phi}{ae}}{1 - \phi}, \qquad \text{(A3)}$$

where $z = 1$ is the counterion valence, $\epsilon = \epsilon_0 \epsilon_r$, ϵ_0 is the permittivity of free space, $\epsilon_r \approx 5.53$ is the dielectric constant of the solvent mixture [73], ρ is the number density of counterions, $\sigma = Ze/4\pi a^2$ is the surface charge density, Z is the total number of charges on a PMMA particle, and ϕ is the volume fraction of particles. The particle charge was estimated as [58]

$$Z = \frac{12a}{\lambda_B}, \qquad \text{(A4)}$$

and the Bjerrum length $\lambda_B \approx 10$ nm was calculated as

$$\lambda_B = \frac{e^2}{k_B T 4\pi\epsilon}. \qquad \text{(A5)}$$

Although most of the parameters are reported in the literature or readily measurable, the counterion concentration ρ needs to be carefully considered. The solubility of TBAC in pure CHB is $260\,\mu$M [74]. Moreover, the degree of dissociation of TBAC is a strong function of the concentration, and is typically 2–3% at high concentrations of salt [74]. Hence, although we used a concentration of TBAC above saturation (1.5 mM), we estimate a counterion concentration of $8\,\mu$M ($\approx 0.03 \times 260\,\mu$M) and use that in the calculation of U_{ES}.

Second, to estimate the depletion potential from a polymer of radius of gyration R_g, we use the form given in Ref. [21], where for $2a \leqslant r \leqslant 2a + 2R_g$ the depletion potential is

$$U_{\mathrm{dep}} = -\Pi_p V_o. \qquad \text{(A6)}$$

In this expression $\Pi_p = n_p k_B T$ is the osmotic pressure of the polymer, n_p is the number density of the polymer in the free volume of solution [21], and

$$V_o = \left\{ 1 - \frac{3r}{2\sigma(1+\xi)} + \frac{1}{2}\left[\frac{r}{\sigma(1+\xi)}\right]^3 \right\} \frac{\pi}{6}\sigma^3(1+\xi)^3 \quad \text{(A7)}$$

is the volume of the overlapping depletion zone between the particles [21]. The resulting interaction potentials contain a deep maximum for the large particles in each series and a weaker maximum for the small particles in each series, as shown in Fig. 10. In each series of experiments the attractive minimum at contact is deeper for the large particles than for the small particles, consistent with a stronger attraction.

[1] B. Derby and N. Reis, MRS Bull. **28**, 815 (2003).

[2] A. M. J. van den Berg, P. J. Smith, J. Perelaer, W. Schrof, S. Koltzenburg, and U. S. Schubert, Soft Matter **3**, 238 (2007).

[3] J. A. Lewis, J. E. Smay, and J. Cesarano, J. Am. Ceram. Soc. **89**, 3599 (2006).

[4] J. A. Lewis, Adv. Funct. Mater. **16**, 2193 (2006).

[5] C. J. Martinez and J. A. Lewis, Langmuir **18**, 4689 (2002).

[6] F. Maximilian, F. Olaf, K. Oliver, and R. Jörg, Nanotechnology **14**, 778 (2003).

[7] J. A. Lewis, J. Am. Ceram. Soc. **83**, 2341 (2000).

[8] A. Vonarbourg, C. Passirani, P. Saulnier, and J.-P. Benoit, Biomaterials **27**, 4356 (2006).

[9] G. Bonacucina, M. Cespi, M. Misici-Falzi, and G. F. Palmieri, J. Pharm. Sci. **98**, 1 (2009).

[10] J. Sarquis, J. Chem. Ed. **57**, 602 (1980).

[11] R. Caenn and G. V. Chillingar, J. Petrol. Sci. Eng. **14**, 221 (1996).

[12] G. C. Maitland, Curr. Opin. Colloid Interface Sci. **5**, 301 (2000).

[13] K. N. Pham, S. U. Egelhaaf, P. N. Pusey, and W. C. K. Poon, Phys. Rev. E **69**, 011503 (2004).

[14] H. Sedgwick, S. U. Egelhaaf, and W. C. K. Poon, J. Phys.: Condens. Matter **16**, S4913 (2004).

[15] C. J. Dibble, M. Kogan, and M. J. Solomon, Phys. Rev. E **74**, 041403 (2006).

[16] Y. Gao and M. L. Kilfoil, Phys. Rev. Lett. **99**, 078301 (2007).

[17] C. J. Dibble, M. Kogan, and M. J. Solomon, Phys. Rev. E **77**, 050401 (2008).

[18] A. P. R. Eberle, N. J. Wagner, and R. Castañeda-Priego, Phys. Rev. Lett. **106**, 105704 (2011).

[19] H. N. W. Lekkerkerker, W. C. K. Poon, P. N. Pusey, A. Stroobants, and P. B. Warren, Europhys. Lett. **20**, 559 (1992).

[20] W. C. K. Poon, A. Pirie, and P. N. Pusey, Faraday Discuss. **101**, 65 (1995).

[21] S. M. Ilett, A. Orrock, W. C. K. Poon, and P. N. Pusey, Phys. Rev. E **51**, 1344 (1995).

[22] V. Prasad, V. Trappe, A. D. Dinsmore, P. N. Segre, L. Cipelletti, and D. A. Weitz, Faraday Discuss. **123**, 1 (2003).

[23] S. A. Shah, Y.-L. Chen, S. Ramakrishnan, K. S. Schweizer, and C. F. Zukoski, J. Phys.: Condens. Matter **15**, 4751 (2003).

[24] J. Bergenholtz, W. C. K. Poon, and M. Fuchs, Langmuir **19**, 4493 (2003).

[25] P. J. Lu, J. C. Conrad, H. M. Wyss, A. B. Schofield, and D. A. Weitz, Phys. Rev. Lett. **96**, 028306 (2006).

[26] S. A. Shah, Y.-L. Chen, K. S. Schweizer, and C. F. Zukoski, J. Chem. Phys. **118**, 3350 (2003).

[27] R. C. Sonntag and W. B. Russel, J. Colloid Interface Sci. **116**, 485 (1987).

[28] C. J. Rueb and C. F. Zukoski, J. Rheol. **41**, 197 (1997).

[29] M. Laurati, G. Petekidis, N. Koumakis, F. Cardinaux, A. B. Schofield, J. M. Brader, M. Fuchs, and S. U. Egelhaaf, J. Chem. Phys. **130**, 134907 (2009).

[30] X. Chu, A. D. Nikolov, and D. T. Wasan, Langmuir **12**, 5004 (1996).

[31] M. Fasolo and P. Sollich, J. Chem. Phys. **122**, 074904 (2005).

[32] S. Rastogi, N. J. Wagner, and S. Lustig, J. Chem. Phys. **104**, 9249 (1996).

[33] P. Sollich and N. B. Wilding, Soft Matter **7**, 4472 (2011).

[34] P. D'Haene and J. Mewis, Rheol. Acta **33**, 165 (1994).

[35] A. D. Dinsmore, A. G. Yodh, and D. J. Pine, Phys. Rev. E **52**, 4045 (1995).

[36] S.-E. Phan, W. B. Russel, J. Zhu, and P. M. Chaikin, J. Chem. Phys. **108**, 9789 (1998).

[37] K. Yoshizawa, N. Wakabayashi, M. Yonese, J. Yamanaka, and C. P. Royall, Soft Matter **8**, 11732 (2012).

[38] T. Sentjabrskaja, E. Babaliari, J. Hendricks, M. Laurati, G. Petekidis, and S. U. Egelhaaf, Soft Matter **9**, 4524 (2013).

[39] J. Hendricks, R. Capellmann, A. B. Schofield, S. U. Egelhaaf, and M. Laurati, Phys. Rev. E **91**, 032308 (2015).

[40] S. Asakura and F. Oosawa, J. Polym. Sci. **33**, 183 (1958).

[41] M. Peláez-Fernández, J. Callejas-Fernández, and A. Moncho-Jordá, Eur. Phys. J. E **35**, 120 (2012).

[42] R. M. L. Evans, D. J. Fairhurst, and W. C. K. Poon, Phys. Rev. Lett. **81**, 1326 (1998).

[43] M. Fasolo and P. Sollich, Phys. Rev. Lett. **91**, 068301 (2003).

[44] A. Imhof and J. K. G. Dhont, Phys. Rev. Lett. **75**, 1662 (1995).

[45] E. Zaccarelli, S. M. Liddle, and W. C. K. Poon, Soft Matter **11**, 324 (2015).

[46] Th. Voigtmann and J. Horbach, Phys. Rev. Lett. **103**, 205901 (2009).

[47] C. Mayer, F. Sciortino, C. N. Likos, P. Tartaglia, H. Löwen, and E. Zaccarelli, Macromolecules **42**, 423 (2009).

[48] D. J. Fairhurst, Polydispersity in Colloidal Phase Transitions, Ph.D. thesis, University of Edinburgh, 1999.

[49] K. N. Pham, A. M. Puertas, J. Bergenholtz, S. U. Egelhaaf, A. Moussaïd, P. N. Pusey, A. B. Schofield, M. E. Cates, M. Fuchs, and W. C. K. Poon, Science **296**, 104 (2002).

[50] S. M. Liddle, T. Narayanan, and W. C. K. Poon, J. Phys.: Condens. Matter **23**, 194116 (2011).

[51] T. H. Zhang, B. W. M. Kuipers, W. Tian, J. Groenewold, and W. K. Kegel, Soft Matter **11**, 297 (2015).

[52] K. N. Pham, G. Petekidis, D. Vlassopoulous, S. U. Egelhaaf, W. C. K. Poon, and P. N. Pusey, J. Rheol. **52**, 649 (2008).

[53] R. Pandey and J. C. Conrad, Soft Matter **9**, 10617 (2013).

[54] L. Antl, J. W. Goodwin, R. D. Hill, R. H. Ottewill, S. M. Owens, S. Papworth, and J. A. Waters, Colloids Surf. **17**, 67 (1986).

[55] M. K. Chow and C. F. Zukoski, J. Rheol. **39**, 15 (1995).

[56] J. C. Crocker and D. G. Grier, J. Colloid Interface Sci. **179**, 298 (1996).

[57] V. Trappe and P. Sandkühler, Curr. Opin. Colloid Interface Sci. **8**, 494 (2004).

[58] C. P. Royall, W. C. K. Poon, and E. R. Weeks, Soft Matter **9**, 17 (2013).

[59] A. Yethiraj and A. van Blaaderen, Nature **421**, 513 (2003).

[60] A.-P. Hynninen and M. Dijkstra, Phys. Rev. E **68**, 021407 (2003).

[61] J. C. Crocker, J. A. Matteo, A. D. Dinsmore, and A. G. Yodh, Phys. Rev. Lett. **82**, 4352 (1999).

[62] The normalized polymer concentration c_p/c_p^*, where c_p^* is the overlap concentration of the polymer, instead increases with increasing ξ, as described in Ref. [26].

[63] J. Bergenholtz and M. Fuchs, Phys. Rev. E **59**, 5706 (1999).

[64] M. Spannuth and J. C. Conrad, Phys. Rev. Lett. **109**, 028301 (2012).

[65] W. Kob, C. Donati, S. J. Plimpton, P. H. Poole, and S. C. Glotzer, Phys. Rev. Lett. **79**, 2827 (1997).

[66] S. A. Shah, Y.-L. Chen, K. S. Schweizer, and C. F. Zukoski, J. Chem. Phys. **119**, 8747 (2003).

[67] N. Koumakis and G. Petekidis, Soft Matter **7**, 2456 (2011).

[68] L. C. Hsiao, M. J. Solomon, K. A. Whitaker, and E. M. Furst, J. Rheol. **58**, 1485 (2014).

[69] S. K. Dutta, A. Mbi, R. C. Arevalo, and D. L. Blair, Rev. Sci. Instrum. **84**, 063702 (2013).

[70] J. Bender and N. J. Wagner, J. Rheol. **40**, 899 (1996).

[71] M. F. Hsu, E. R. Dufresne, and D. A. Weitz, Langmuir **21**, 4881 (2005).

[72] J. Eastman, in *Colloid Science Principles, Methods and Applications*, edited by T. Cosgrove (John Wiley & Sons, Ltd., Chichester, 2010), Chap. 3, pp. 45–60.

[73] P. Wang and A. Anderko, Fluid Phase Equilib. **186**, 103 (2001).

[74] M. E. Leunissen, Manipulating Colloids with Charges & Electric Fields, Ph.D. thesis, Universiteit Utrecht, 2007.